Available online at www.sciencedirect.com
ScienceDirect
Journal of the European Ceramic Society 26 (2006) 3681–3686
www.elsevier.com/locate/jeurceramsoc

The low-temperature formation of barium hexaferrites

Darja Lisjak *, Miha Drofenik

Jožef Stefan Institute, Advanced Materials Department, Jamova 39, Ljubljana, Slovenia

Received 7 September 2005; received in revised form 1 December 2005; accepted 9 December 2005
Available online 17 February 2006

Abstract

We have investigated the formation of barium hexaferrites with the compositions $BaFe_{12}O_{19}$ and $Ba_2Co_2Fe_{12}O_{22}$ using precipitation in ethanol. A mechanism for the formation was proposed, based on the results of thermal analysis, X-ray powder diffraction, electron microscopy and the magnetic properties of powders prepared under various precipitation and calcination conditions. The influence of the precipitation conditions on the formation mechanism and the reaction rate was studied. By replacing the water with ethanol the formation temperatures of both compounds were decreased to well below 1000 °C, and the homogeneity of their microstructures was improved. As a result, homogeneous and dense ceramics were obtained at 1200 °C. Precipitation from ethanol solutions proved to be a simple method for the low-temperature preparation of barium hexaferrites.

Keywords: Powders-chemical preparation; Magnetic properties; Ferrites; Hexaferrites; $BaFe_{12}O_{19}$

1. Introduction

Barium hexaferrite and its derivatives can be used for permanent magnets, magnetic-recording media and microwave applications because of their specific magnetic properties. As a result of their high anisotropy fields hexaferrites can be used at much higher frequencies than spinel ferrites or garnets.[1,2] Therefore, M-type hexaferrites, that possess uniaxial magnetocrystalline anisotropy can also be used for mm-wave applications. While Y-type hexaferrites, which possess a planar magnetocrystalline anisotropy, are promising materials for microwave absorbers. Barium hexaferrite, with its chemical formula $BaFe_{12}O_{19}$ (the so-called M-type or shortly BaM), is the best-known representative of the hexaferrite family. Its crystal structure is the so-called magnetoplumbite structure; this can be described as a stacking sequence of the basic blocks S and R.[3] Y-type hexaferrites have the chemical formula $Ba_2Me_2Fe_{12}O_{22}$ (Me = bivalent transition-metal ion). Their crystal structure can be described as a stacking sequence of S and T basic blocks.[3]

Low-loss materials for microwave applications need to be defect free from the compositional, structural and microstructural points-of-view. Finer starting powders tend to exhibit a superior sintering behaviour, resulting in a lower sintering temperature and denser ceramics when compared to coarser powders.[4] The formation of barium hexaferrites normally involves the decomposition of $BaCO_3$, which determines the minimum temperature for M-hexaferrite formation. $BaCO_3$ is either present in the initial reaction mixture (solid-state reaction, high-energy milling)[5–7] or is formed from precursors during the preparation process (coprecipitation, organic-precursor reaction).[8–10] The formation of $BaFe_2O_4$ (barium monoferrite) and M-hexaferrite starts after the degradation of the $BaCO_3$ at 700–900 °C.[11–13] The formation of the Y-type hexaferrites starts at ≥1000 °C.[13,14] The preparation methods with, which the formation of $BaCO_3$ was more or less successfully prevented are based on relatively complex procedures.[14–17]

Here we report on a simple precipitation method for the preparation of fine barium hexaferrite powders. In order to suppress the $BaCO_3$ formation we replaced the water with ethanol, in which the solubility of CO_2 from the air is negligible. We studied the influence of various parameters on $BaFe_{12}O_{19}$ formation and correlated these parameters with the reaction kinetics. Finally, we applied the obtained findings to the preparation of the Y-type hexaferrite, $Ba_2Co_2Fe_{12}O_{22}$. Microstructurally homogeneous $Ba_2Co_2Fe_{12}O_{22}$ ceramics were prepared from the calcined powders.

2. Experimental procedure

Samples with compositions $BaFe_{12}O_{19}$ (BaM) and $Ba_2Co_2Fe_{12}O_{22}$ (Co_2Y) were prepared using precipitation

* Corresponding author. Tel.: +386 1 4773872; fax: +386 1 4773875.
E-mail address: darja.lisjak@ijs.si (D. Lisjak).

0955-2219/$ – see front matter © 2006 Elsevier Ltd. All rights reserved.
doi:10.1016/j.jeurceramsoc.2005.12.014

Table 1
Precipitation conditions for hexaferrite samples

Sample	Type of precipitation	Reagent salts	Precipitation atmosphere
MCl	Coprecipitation	$BaCl_2$, $FeCl_3$	Air
MCl–Ar	Coprecipitation	$BaCl_2$, $FeCl_3$	Ar
M	Precipitation	$Ba(CH_3COO)_2$, $FeCl_3$	Air
M–Ar	Precipitation	$Ba(CH_3COO)_2$, $FeCl_3$	Ar
Y	Precipitation Ba, Fe + Co	$Ba(CH_3COO)_2$, $FeCl_3$, $Co(CH_3COO)_2$	Air
Y–Ar	Precipitation Ba, Fe + Co	$Ba(CH_3COO)_2$, $FeCl_3$, $Co(CH_3COO)_2$	Ar

under the various conditions listed in Table 1. Solutions of stoichiometric amounts of $BaCl_2$ (Alfa produkte) and $FeCl_3$ (Alfa Aesar) salts in an ethanol/water solution with a volume ratio of 3:1 were coprecipitated with NaOH (Alfa Aesar) at pH 13, normally in air or under a constant flow of Ar (samples MCl and MCl–Ar, respectively). In the case of the M, M–Ar, Y and Y–Ar samples, $FeCl_3$ (Alfa Aesar) and $Co(CH_3COO)_2$ (Ventron) were dissolved together in an ethanol/water solution with a volume ratio of 3:1. The Fe^{3+} and Co^{2+} were simultaneously precipitated with NaOH at pH 13, while Ba^{2+} from the $Ba(CH_3COO)_2$ (Alfa Aesar) ethanol/water solution was precipitated separately. Afterwards, all the precipitates were mixed together. The precipitated precursors were washed with ethanol and dried at approximately 80 °C and finally calcined at 300–1100 °C for 0–50 h. The calcined powders were washed with water in order to dissolve the NaCl, which was a side product of the precipitation. The powders were sintered at 1200 °C.

The synthesis was monitored with thermogravimetric and differential thermogravimetric analyses (TGA and DTA) using a Netzsch STA 429 TG/DT analyser, and X-ray powder diffraction (XRD) using a D4 Endeavor diffractometer, Bruker AXS. The activation energy (E_a) of the powders was determined from the DTA scans taken at heating rates (h) of 2–15 K/min using the relationship in Eq. (1).[18,19] Here, T_m is the temperature of the DTA peak corresponding to the barium hexaferrite formation and C' is a constant.

$$\log h = -\frac{E_a}{4.57}\frac{1}{T_m} + C'. \quad (1)$$

The development of the powders' microstructures was observed using a Jeol-2000FX transmission electron microscope (TEM). The DC magnetic properties of the powders were measured using a Drusch & Cie Voltreg 1.4 T magnetometer with a maximum magnetic field of 1.2 T.

3. Results and discussion

3.1. Characterization of M-hexaferrite samples

Fig. 1 shows TEM micrographs of the MCl samples. Platelike particles of BaM with diameters of 50–80 nm, surrounded with an amorphous phase, were observed in the powder calcined at 500 °C for 10 h. The number of observed BaM particles increased and the amount of amorphous phase decreased with the increasing calcination temperature. An example is shown in the TEM micrograph of the MCl sample calcined at 700 °C for 1 h. As can be seen, the particles are of approximately the same size in both samples (see Fig. 1).

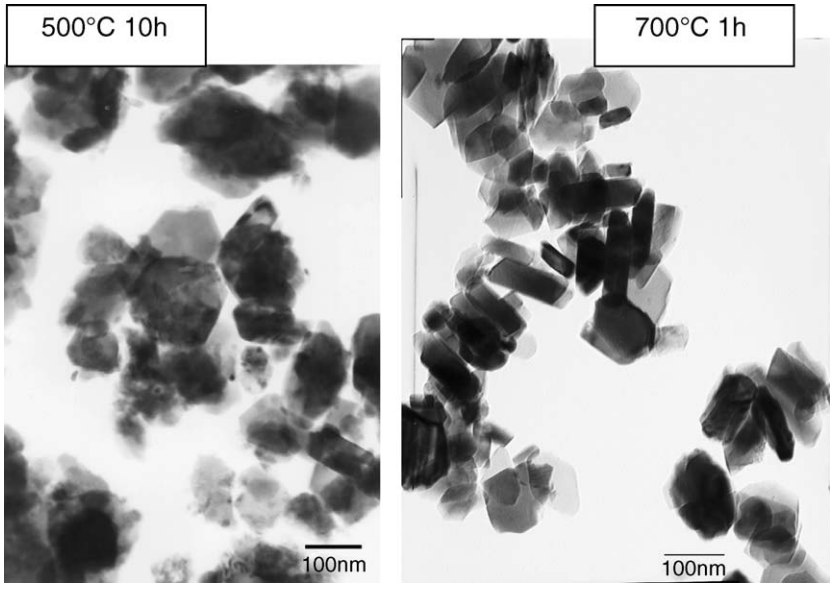

Fig. 1. TEM micrographs of MCl samples calcined at 500 °C for 10 h and 700 °C for 1 h.

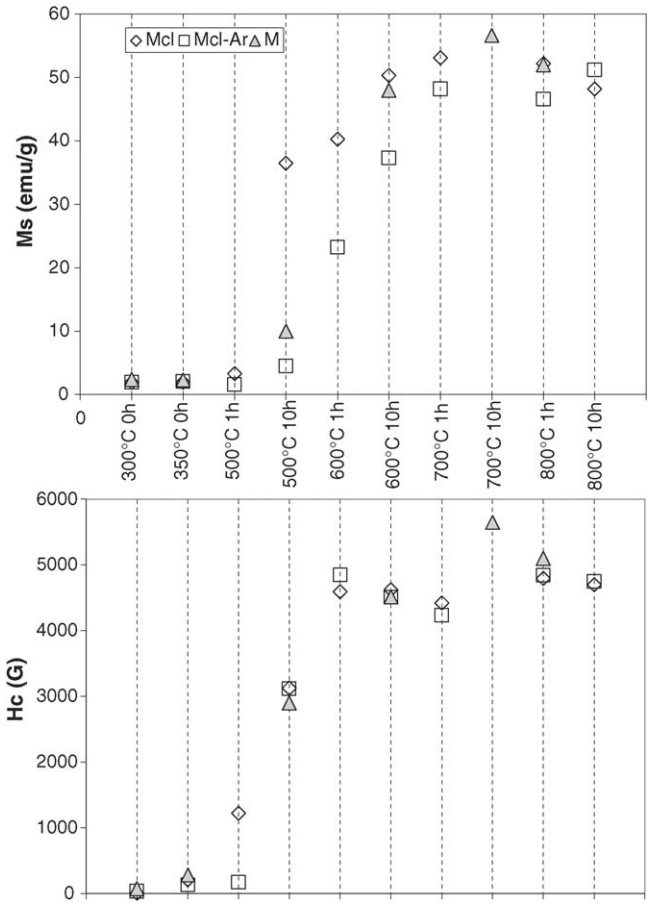

Fig. 2. Saturation magnetization measured at 1.2 T (Ms) and coercivity (Hc) of the $BaFe_{12}O_{19}$ samples.

Fig. 2 shows the magnetization measured at 1.2 T (Ms) and the coercivity (Hc) of the M samples calcined at different temperatures. The Ms and Hc increased in a similar way for individual samples with increasing calcination temperatures and times. In the case of the MCl and MCl–Ar samples, both values were negligible below 500 °C and increased significantly up to 600 °C. After that the Ms and Hc increased only slightly with a further increase in calcination temperature. For the M samples the Ms and Hc increased significantly to 700 °C. From this we could conclude that the majority of the BaM phase formed up to 600 °C in the MCl and MCl–Ar samples, and up to 700 °C in the M samples. The maxiumum Ms values of all three samples were lower than those reported previously for the BaM prepared with coprecipitation (>60 emu/g).[11,12] However, the reported Ms values were measured at higher applied field (1.6 T) than in this study (1.2 T). The applied field of 1.2 T was not high enough to completely saturate the samples due to their high magnetocrystalline anisotropy field.[3] On the other hand the maximum Hc values of 4800–5700 Oe are similar to those obtained by others.[11,12]

The formation of BaM in the MCl samples can be seen in the X-ray diffractograms shown in Fig. 3. Even at as low as 500 °C the main crystalline phase in the sample was BaM. A minor hematite peak indicates that the sample was not single phase. In addition, the relatively high intensity of the peak at $2\theta \sim 35.8°$ could be the result of a small amount of maghemite.

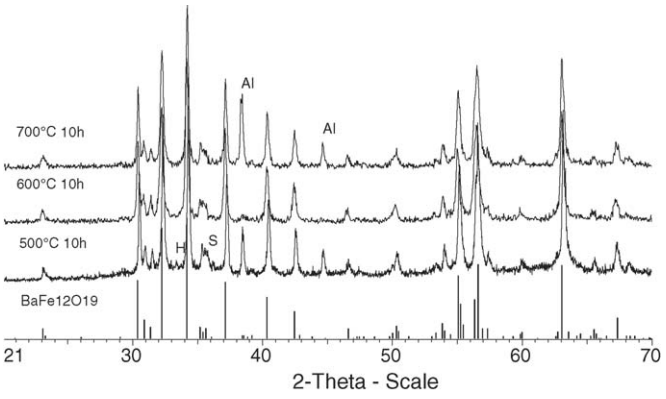

Fig. 3. X-ray diffractograms of MCl samples calcined for 10 h at 500–700 °C. H denotes hematite, S denotes maghemite and Al denotes aluminium from the sample holder. Below is a standard diffraction pattern (μPDSM No. 84-0757) for the $BaFe_{12}O_{19}$ structure.

When the calcination temperature was increased to 600 °C and above, only BaM was detected with the XRD. This is consistent with the magnetic measurements discussed above. Similar formation steps, albeit under different calcination conditions, were also observed for the MCl and M–Ar samples. BaM, as the only crystalline phase, was detected in the MCl–Ar sample calcined at 500 °C for 10 h and in the M–Ar sample calcined at 700 °C for 10 h. The formation of BaM in the M sample also involved the formation of $BaFe_2O_4$ prior to the completed formation of BaM. In the M sample BaM was first detected when calcined at 600 °C for 1 h and was the only crystalline phase when calcined at as high as 800 °C for 3 h. The formation temperature of the BaM was decreased by replacing water, as the solvent, with an ethanol solution.

The TGA and DTA curves for the M and M–Ar samples measured up to 1000 °C with a heating rate of 10 K/min are shown in Fig. 4. There was no significant difference between the curves of each sample. A mass loss is detected up to 600–700 °C; this is associated with the loss of water and CO_2 during the degradation of the as-precipitated precursors. The endothermic peak with a minimum at 80–170 °C is associated with the loss of water, and is accompanied by a mass loss of approximately 20%. The mass continues to decrease with temperature up to 630–680 °C; this can be associated with the additional loss of water as well as the loss of CO_2 due to the degradation of precursors (hydroxide and hydrates, acetate and carbonate groups). Two minor exothermic peaks can be seen in the DTA curve at 298 °C for both samples and at 345 and 355 °C for the M and M–Ar samples, respectively. According to the XRD analysis these two peaks most probably correspond to the crystallization of hematite and maghemite. The most pronounced exothermic DTA peak was detected at 683 and 673 °C for the M and M–Ar samples, respectively; this is associated with the formation of BaM. At these temperatures only a negligible amount of mass loss (up to 0.4%) was detected. The heating rate significantly influenced the formation of BaM. An exothermic peak in the DTA curve, associated with the crystallization of BaM, was detected between 652–693 and 642–684 °C for various heating rates for the M and M–Ar samples, respectively. The temperatures of the DTA peaks decreased with the

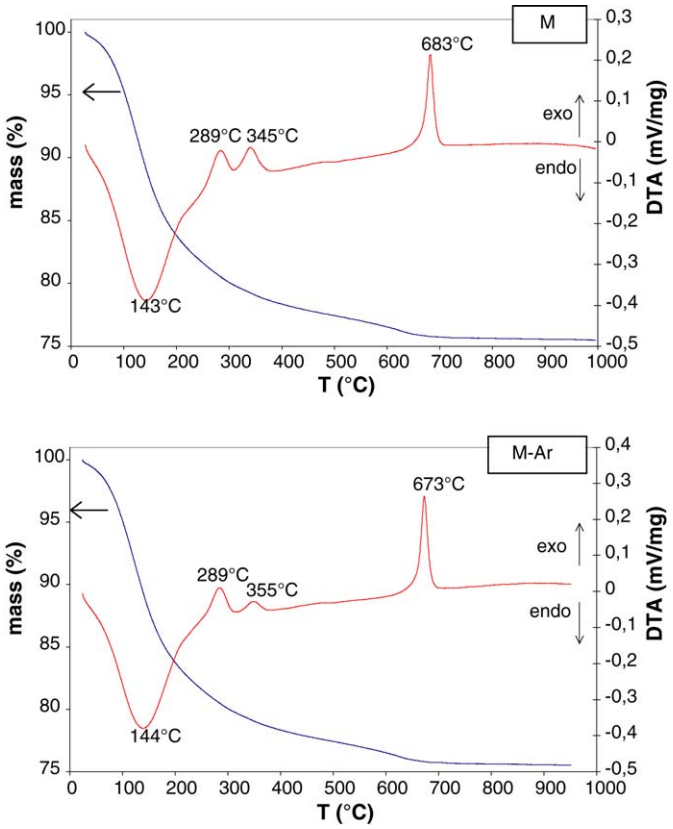

Fig. 4. TGA and DTA curves of the M and M–Ar samples measured at a heating rate 10 K/min.

decreasing heating rates. This confirmed that the crystallization of BaM was strongly kinetically dependent and that the crystallization rate was higher for the M–Ar sample than for the M sample. Furthermore, BaM crystallized when the M and M–Ar samples were calcined for ≥1 h at as low as ≥600 °C (see previous discussion). The linear dependence of $\log h$ versus $1/T_m$ is shown in Fig. 5, where h is the heating rate and T_m is the temperature of the DTA peak's maximum. The activation energy (E_a) for the BaM crystallization was calculated from the curve's slope

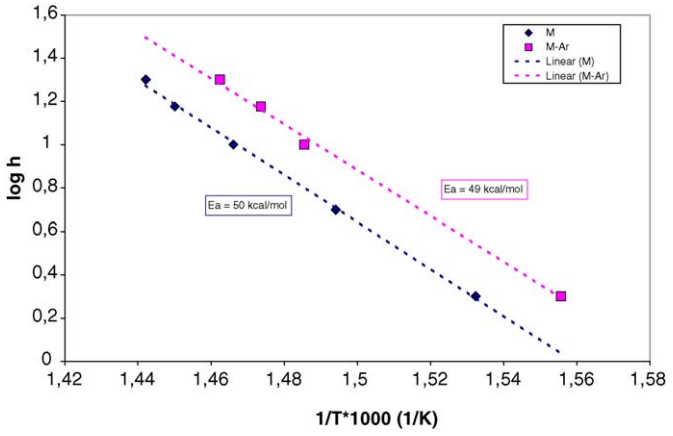

Fig. 5. Determination of the activation energy for the $BaFe_{12}O_{19}$ formation in the M and M–Ar samples according to Eq. (1), where h is the heating rate and Tm is the temperature of the DTA peak's maximum.

using Eq. (1), and was approximately 50 kcal/mol for both samples. E_a is by definition the minimum kinetic energy required for the reactants in order to form products.[20] Finally, we are able to conclude that the chemical processes involved in the crystallization of BaM were the same, regardless of the precipitation gas (air or Ar).

3.2. Formation of $BaFe_{12}O_{19}$

Based on the magnetic properties, the XRD and TGA/DTA analyses we can describe the general mechanism of BaM formation from the precipitated precursors as follows:

$$(1-v)\text{Ba-precursor}(a) + v\text{BaCO}_3 + \text{Fe-precursor}(a) \xrightarrow{T_1,-\text{H}_2\text{O(g)},-\text{CO}_2\text{(g)}} 5\left(1-z-\frac{6}{5}u\right)\text{Fe}_2\text{O}_3(\alpha) + 6u\text{Fe}_2\text{O}_3(\gamma) + (1-z)\text{BaFe}_2\text{O}_4 + z\text{BaFe}_{12}\text{O}_{19} \quad (2)$$

$$u\text{Fe}_2\text{O}_3(\gamma) \xrightarrow{T_2} u\text{Fe}_2\text{O}_3(\alpha) \quad (3)$$

$$5(1-z)\text{Fe}_2\text{O}_3(\alpha) + (1-z)\text{BaFe}_2\text{O}_4 \xrightarrow{T_3} (1-z)\text{BaFe}_{12}\text{O}_{19} \quad (4)$$

The amorphous phases are marked with (a); all the other phases are crystalline. (α) and (γ) correspond to α-Fe_2O_3 (hematite) and γ-Fe_2O_3 (maghemite), respectively. Note that the variables u, v, z, x, y are in the range 0–1. The temperatures and the variables in Eqs. (2)–(4) depend on the preparation conditions: the type of reagent salts, the precipitation atmosphere, the aging of the precipitates, the temperature and the time of calcination. Although in fresh precipitates no $BaCO_3$ was detected with the XRD analysis or observed with the TEM, this was not true for the precipitates exposed to air for a day or more. This clearly suggests that the amorphous Ba-precursor reacted with the CO_2 in the air. When the precipitation was carried out in Ar or from chlorides, no intermediate phase, $BaFe_2O_4$, was formed ($z = 1$). This could be explained by the enhanced diffusion rate due to the flux of NaCl (a side product of the coprecipitation from chlorides) and by the improved homogeneity of the precipitates due to additional stirring by the Ar flow. Consequently, T_1 was the lowest for the MCl and MCl–Ar samples (500 °C); for the M and M–Ar the T_1 was 600 °C. T_2 was equal to 600 °C for all the samples, while $T_3 \geq 600$ °C for the M sample.

Fig. 6 shows X-ray diffractograms of the MCl sample calcined at 500 °C for 50 h. Here, the X-ray diffractogram of the as-fired sample is shown in order to prove that the BaM formation was promoted in the presence of NaCl. Peaks corresponding to the $BaFe_{12}O_{19}$ and NaCl (rocksalt) structures can be observed. Obviously, BaM can be formed directly, following Eq. (2) with $z = 1$. As discussed previously, the same was true for the MCl–Ar sample calcined at 500 °C for only 10 h. Clearly, the Ar flow used during the precipitation additionally enhanced the formation rate of BaM. Here we have shown that the BaM formation temperature was reduced to 500 °C by increasing its formation rate using appropriate preparation conditions.

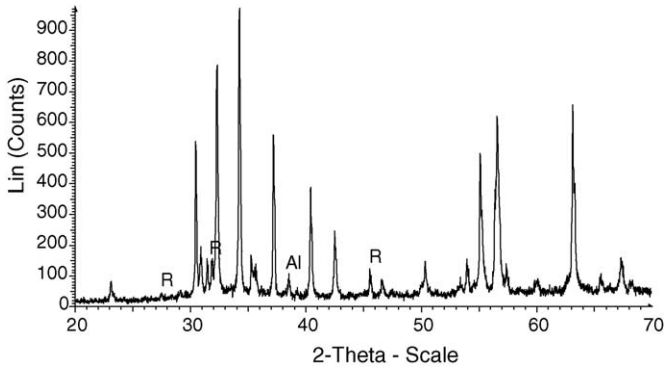

Fig. 6. X-ray diffractogram of the MCl sample calcined at 500 °C for 50 h. R denotes NaCl and Al denotes aluminium from the sample holder. Unmarked peaks correspond to the $BaFe_{12}O_{19}$ structure (see also Fig. 3).

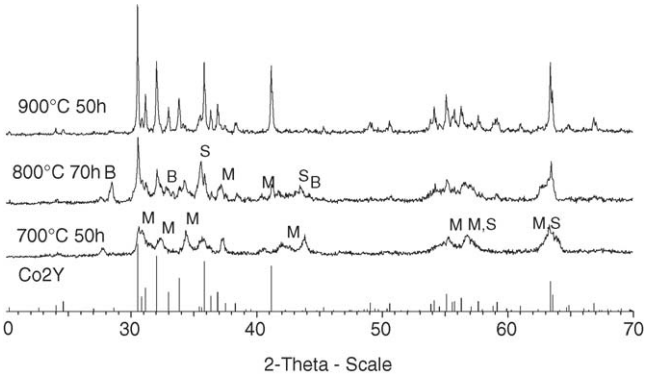

Fig. 7. X-ray diffractograms of Y–Ar samples. M denotes M-hexaferrite, B denotes $BaFe_2O_4$, and S denotes $CoFe_2O_4$. Below is a standard diffraction pattern (μPDSM No. 82-0472) for the $Ba_2Co_2Fe_{12}O_{22}$ structure.

3.3. Formation of Co_2Y hexaferrite

We tried to apply the same method for the preparation of Co_2Y bacause it is more interesting for applications in the low-GHz region than BaM. Crystalline phases detected in differently calcined samples with XRD analysis are listed in Table 2. Similar to the BaM, $BaCO_3$ was detected in the precipitates that were exposed to the air for longer time. $BaCO_3$ was the only crystalline phase detected in the samples calcined up to 400 °C. Hematite and $BaFe_2O_4$ were detected in the samples calcined at minimum 600 °C while $CoFe_2O_4$ (Co spinel) was detected in the samples calcined at 680 °C. In the samples calcined at higher temperatures $BaFe_2O_4$, $CoFe_2O_4$, BaM and Co_2Y were detected. This can be also seen in the diffractograms shown in Fig. 7. Peaks corresponding to the Y- and M-hexaferrite, barium monoferrite and spinel structures can be observed in the diffractogram of the Y–Ar samples calcined at 700 and 800 °C for a longer period. This indicates that Co_2Y started to form at as low as 700 °C, which is several hundreds °C lower than usually reported for coprecipitation from water solutions.[13] The intensities of the Y-hexaferrite peaks increase with the calcination temperature at the expense of the other peaks' intensities; at the same time the background level is decreasing. The Co_2Y formation was complete after 50 h calcination at 900 °C or 10 h calcination at 1000 °C. The Co_2Y formation in the Y sample was completed at a higher temperature, i.e. 1100 °C. Again, Ar enhanced the reaction rate. Based on the XRD analysis the formation of Co_2Y can be roughly written as follows:

$$(1-v)\text{Ba-precursor}(a) + v\text{BaCO}_3 + \text{Fe-precursor}(a) + \text{Co-precursor}(a) \overset{600-680\,^\circ\text{C}, -\text{H}_2\text{O(g)}, -\text{CO}_2\text{(g)}}{\longrightarrow} 2\text{BaFe}_2\text{O}_4 + 2\text{Fe}_2\text{O}_3(\alpha) + 2\text{CoFe}_2\text{O}_4 \quad (5)$$

$$\overset{700\,^\circ\text{C}}{\longrightarrow}(1-z)\text{Ba}_2\text{Co}_2\text{Fe}_{12}\text{O}_{22} + \tfrac{2}{5}z\text{BaFe}_{12}\text{O}_{19} + \tfrac{8}{5}z\text{BaFe}_2\text{O}_4 + 2z\text{CoFe}_2\text{O}_4 \quad (6)$$

$$\overset{900-1100\,^\circ\text{C}}{\longrightarrow}\text{Ba}_2\text{Co}_2\text{Fe}_{12}\text{O}_{22} \quad (7)$$

A huge background, which increased with the calcination temperature, was observed in the X-ray diffractograms of the samples calcined up to 800 °C. This indicated the presence of an amorphous phase. For the sake of clarity the leftover amorphous phase was neglected in Eqs. (5)–(7). The temperature interval for the reaction (7) is related to different reaction temperatures with the respect to the precipitation atmosphere (air or Ar). Regardless of the precipitation or calcination conditions, Co_2Y was

Table 2
Crystalline phases detected in differently calcined Y and Y–Ar samples

Calcination temperature (°C)	Calcination time (h)	Y	Y–Ar
/	Fresh precipitates	/	/
/	Old precipitates	W	W
400	0	W	W
600	3	W, B, H	W, B, H
680	0	B, H, S	B, H, S
700	10	B, S, M, Y	B, S, M, Y
700	50	B, S, M, Y	B, S, M, Y
800	70	B, S, M, Y	B, S, M, Y
900	50	B, S, M, Y	Y
1000	10	B, Y	Y
1100	3	Y	Y

W denotes witherite ($BaCO_3$), B denotes barium monoferrite ($BaFe_2O_4$), H denotes hematite (α-Fe_2O_3), S denotes spinel ($CoFe_2O_4$), M denotes BaM ($BaFe_{12}O_{19}$) and Y denotes Co_2Y ($Ba_2Co_2Fe_{12}O_{22}$).

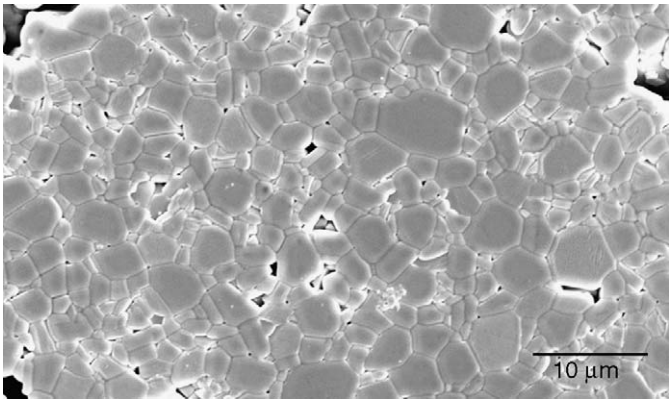

Fig. 8. SE image of the $Ba_2Co_2Fe_{12}O_{22}$ ceramics sintered at 1200 °C for 3 h.

not formed directly, like in the case of the BaM, but it was formed via intermediates like in the case of other preparation methods.[13,14]

Fig. 8 shows a secondary-electron image (SEI) of the etched surface of Co_2Y ceramics sintered at 1200 °C, prepared from the Y–Ar sample. Samples with a minimum relative density of 90% and a relatively homogeneous microstructure were obtained at 1200 °C without any sintering aids. These ceramics showed interesting microwave properties in the low-GHz region.[21]

4. Conclusions

We studied the formation of $BaFe_{12}O_{19}$ and $Ba_2Co_2Fe_{12}O_{22}$ using coprecipitation in ethanol solutions. The formation of $BaFe_{12}O_{19}$ involves two competing mechanisms: (i) direct formation from amorphous precursors and (ii) formation via crystalline intermediates. The first mechanism occurred at much lower temperatures than the second one. This resulted in a very low initial formation temperature of 500 °C, and a higher temperature, i.e. 500–800 °C, or a longer time required for the complete formation. The overall formation mechanism did not change, although the reaction rate was greatly affected by the preparation conditions. The formation of $Ba_2Co_2Fe_{12}O_{22}$ was not straightforward in any case, since it was formed from the intermediates $BaFe_{12}O_{19}$, $BaFe_2O_4$ and $CoFe_2O_4$. Nevertheless, its formation started at a relatively low temperature of 700 °C and was completed at 900–1100 °C depending on the precipitation atmosphere (air or Ar). Powders prepared in this way can be sintered at 1200 °C without any sintering aids.

Acknowledgements

This work was supported by The Ministry of Education, Science and Sports of the Republic of Slovenia and the company Iskra Feriti.

References

1. Pardavi-Horvath, M., Microwave Applications of Soft Ferrites. *J. Magn. Magn. Mater.*, 2000, **215–216**, 171–183.
2. Jonker, G. H., Wijn, H. P. K. and Braun, P. B., Feroxplana, hexagonal ferromagnetic iron-oxide compounds for very high frequencies. *Philips Technol. Rev.*, 1956, **18**, 145–180.
3. Smit, J. and Wijn, H. P. J., *Ferrites*. Philips' Technical Library, Eindhoven, 1959, Chapter IX.
4. Rozman, M. and Drofenik, M., Sintering of nanosized MnZn-ferrite powders. *J. Am. Ceram. Soc.*, 1998, **81**, 1757–1763.
5. Goto, Y. and Takada, T., Phase diagram of the system $BaO–Fe_2O_3$. *J. Am. Ceram. Soc.*, 1960, **43**, 150–153.
6. Sloccari, G., Phase equilibrium in the subsystem $BaO·Fe_2O_3–BaO·6Fe_2O_3$. *J. Am. Ceram. Soc.*, 1973, **56**, 489–490.
7. Ding, J., Maurice, D., Miao, W. F., McCormick, P. G. and Street, R., Hexaferrite magnetic materials prepared by mechanical alloying. *J. Magn. Magn. Mater.*, 1995, **150**, 417–420.
8. Carp, O., Barjega, R., Segal, E. and Brezeanu, M., Nonconventional methods for obtaining hexaferrites II.barium hexaferrite. *Thermochim. Acta*, 1998, **318**, 57–62.
9. Zhong, W., Ding, W., Zhang, N., Hong, J., Yan, Q. and Du, Y., Key step in synthesis of ultrafine $BaFe_{12}O_{19}$ by sol–gel technique. *J. Magn. Magn. Mater.*, 1997, **168**, 196–202.
10. Ng, W. K., Ding, J., Chow, Y. Y., Wang, S. and Shi, Y., A study on barium ferrite particles prepared by chemical coprecipitation. *J. Mater. Res.*, 2000, **15**, 2151–2156.
11. Ross, W., Formation of chemically coprecipitated barium ferrite. *J. Am. Ceram. Soc.*, 1980, **63**, 601–603.
12. Haneda, K., Miyakawa, C. and Kojima, H., Preparation of high-coercitivity $BaFe_{12}O_{19}$. *J. Am. Ceram. Soc.*, 1974, **57**, 354–357.
13. Haijun, Z., Xi, Y. and Liangying, Z., The preparation and microwave properties of $Ba_2Zn_zCo_{2-z}Fe_{12}O_{22}$ hexaferrites. *J. Eur. Ceram. Soc.*, 2002, **22**, 835–840.
14. Pullar, R. C., Taylor, M. D. and Bhattacharya, A. K., Magnetic Co_2Y ferrite, $Ba_2Co_2Fe_{12}O_{22}$ fibres produced via a blow spun process. *J. Mater. Sci.*, 1997, **32**, 365–368.
15. Sudakar, C., Subbannna, G. N. and Kutty, T. R. N., Nanoparticles of barium hexaferrite by gel to crystalline conversion and their magnetic properties. *J. Electroceram.*, 2001, **6**, 123–134.
16. Pullar, R. C. and Bhattacharya, A. K., Crystallization of hexagonal M ferrites from a stoichiometric sol–gel precursor, without formation of the α-$BaFe_2O_4$ intermediate phase. *Mater. Lett.*, 2002, **57**, 537–542.
17. Ogasawara, T. and Oliviera, M. A. S., Microstructure and hysteresis curves of the barium hexaferrite from co-precipitation by organic agent. *J. Magn. Magn. Mater.*, 2000, **217**, 147–154.
18. Kulkarni, S. D., Deshpande, C. E., Shrotri, J. J., Gunjikar, V. G. and Date, S. K., Thermochemical characterization of ultrafine Sr-hexaferrite. *Thermochim. Acta*, 1989, **153**, 47–61.
19. Maritta, A. and Buri, A., Kinetics of devitrification and differential thermal analysis. *Thermochim. Acta*, 1978, **25**, 155–160.
20. Atkins, P. W., *Physical Chemistry*. Oxford University Press, New York, 1998, pp. 775–777.
21. Lisjak, D. and Drofenik, M., The preparation of single-domain barium hexaferrites using coprecipitation in ethanol. In *Proceedings of the Ninth International Conference on Ferrites (ICF-9)*, ed. R. F. Soohoo, 2004, pp. 665–670.